Applied Catalysis B: Environmental 224 (2018) 1017–1026

Contents lists available at ScienceDirect

Applied Catalysis B: Environmental

journal homepage: www.elsevier.com/locate/apcatb

Research paper

Electrocatalytic oxidation of formaldehyde on nanoporous nickel phosphate modified electrode

A.H. Touny[b,c], Reham H. Tammam[a], M.M. Saleh[a,c,*]

[a] Department of Chemistry, Faculty of Science, Cairo University, Cairo, Egypt
[b] Department of Chemistry, Faculty of Science, Helwan University, Helwan, Egypt
[c] Department of Chemistry, College of Science, King Faisal University, Al-Hassa, Saudi Arabia

ARTICLE INFO

Keywords:
Nickel
GC
Phosphate
Formaldehyde
Nanoporous

ABSTRACT

Nanoporous nickel phosphate (nano-NiPh) is synthesized using a hydrothermal-based method from nickel phosphate precursors. It is applied for electrocatalytic oxidation of formaldehyde (FAL) in alkaline solution. The produced material is characterized using different techniques such as field emission scanning electron microscopy (FE-SEM), transmission electron micrograph (TEM) and X-ray diffraction (XRD) pattern. The nano-NiPh particles nearly reveal one-dimensional nanosize (200 × 800 nm) and demonstrate nanopores of ~30 nm size. The chemical identity is found to be $Ni_3(PO_4)_2.8H_2O$. A nano-NiPh modified glassy carbon electrode (GC/nano-NiPh) is characterized by various techniques including cyclic voltammetry (CV), chronoamperometry and electrochemical impedance spectroscopy (EIS). The fabricated electrode demonstrates significant electrocatalytic activity towards the electrochemical oxidation of formaldehyde. The activity and stability of the electrode are discussed and some transport and kinetic parameters for FAL electrochemical oxidation have been determined.

1. Introduction

Electrochemical oxidation of formaldehyde is considered to be a dual-function process. In one side, it serves as analogy to formic acid as a fuel in what is so called direct formic acid fuel cell (DFAFC) [1]. In the other side, it can be used as a method for removing and/or conversion of formaldehyde to less toxic species from dilute waste streams [2–4]. However, the choice of the electrode catalyst with a superior design and composition for such anodic reaction is considered to be an important issue. Usually, Pt and Pt-based electrocatalysts have been used for electrochemical oxidation of formaldehyde [5,6] and formic acid as well [7–9]. Since those Pt-based electrodes are suffering mainly from poisoning and are costly [8,9], therefore there is an obvious reason for finding new catalysts for such important reaction. This can be accomplished by replacement of Pt-based catalysts either partially or totally.

In literatures, nickel and nickel oxide-based materials have been applied several times as electrocatalysts and their high catalytic activity towards electrochemical oxidation of small organic compounds are well documented [10–18]. Of these organic molecules, formaldehyde electrooxidation is considered to be one of the significant applications for Ni-based electrocatalysts. Roof et al. [19], used nickel particles electrodeposited onto poly(m-toluidine), Yu et al. [20], utilized nickel ion implanted-modified indium tin oxide electrode (NiNPs/ITO). Ciszewski et al. [21], used nickel porphyrin-based glassy carbon electrode, Ojani et al. [22], applied nickel modified ionic liquid carbon paste electrode, Monfared et al. [23], used poly(*N*-methylaniline)/nickel modified carbon paste electrode. Hassaninejad–Darzi et al. [24], used nickel ions dispersed onto chitosan-modified carbon paste electrode, Jiao et al. [25], used planar nickel electrode and Dong et al. [26], used $Ni(OH)_2$/Ni. In all of the above catalysts the redox couple $Ni(OH)_2$/NiOOH has been found to play an essential role to mediate the electrochemical oxidation of formaldehyde on such electrodes. The present work can be considered as a first trial to use NiPh modified electrode as an electrocatalyst for oxidation of FAL. The NiPh is bearing a redox couple (NiPh(II)/NiPh(III)) after electrochemical activation in alkaline electrolyte and the phosphate structure can offer stability of the redox couple due to its stable matrix. Using NiPh in electrocatalysis can be considered as scarce [27].

Metal phosphates (NiPh) have displayed many academic interests and technological applications due to its unique chemical structure and reactivity for different physicochemical processes [28,29]. Of these substantial applications are; catalysis in chemical conversions [30,31], tissue engineering [32,33], drug delivery [34] and antibacterial activity [35,36]. Also, they have been used in lithium batteries [37,38], supercapacitors [39,40], catalytic [41] and electrocatalytic reactions [42]. The literatures have cited many approaches for the synthesis of

* Corresponding author.
E-mail addresses: mahmoudsaleh90@yahoo.com, mmsaleh@kfu.edu.sa (M.M. Saleh).

https://doi.org/10.1016/j.apcatb.2017.11.031
Received 19 August 2017; Received in revised form 9 November 2017; Accepted 14 November 2017
Available online 17 November 2017

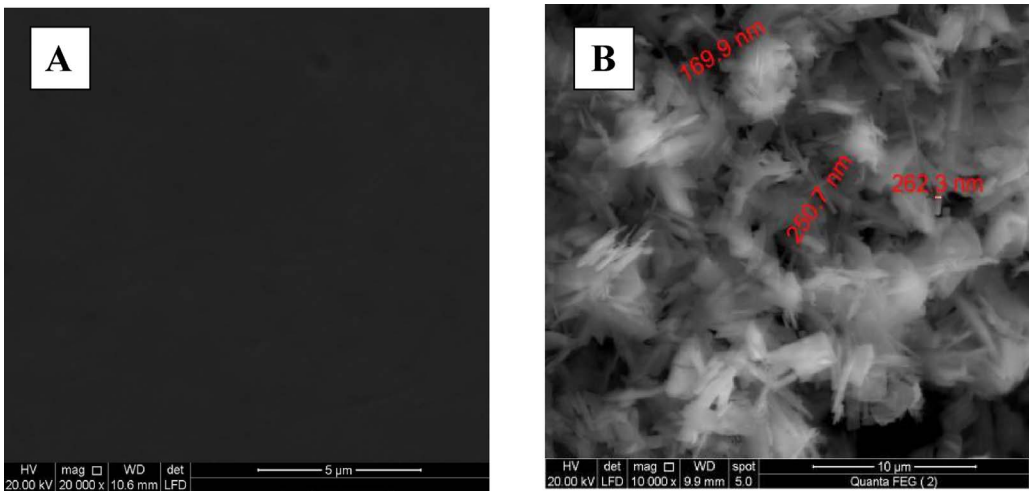

Fig. 1. SEM image of bare GC (A) and NiPh/GC (B).

nickel phosphates. These include (but not limited to): solvothermal [43,44], hydrothermal [45], wet chemical process [46,47] and sol-gel technique [48]. The fabrication route can determine the chemical composition, structural and morphological properties.

According to the literatures, it has been found that the properties of the formed materials are mainly influenced by the fabrication methods and consequently these materials can be used in various applications [49]. Fabrication of nickel phosphate particles with different morphological size (in nano- and micro scales) using surfactants, ligands or solid membrane templates has been found in literatures [50]. The hydrothermal process is mainly known as an eco-friendly technique and calcination step is maybe required. However, it has two major disadvantages: time consuming and not cost-effective [51]. Therefore creating an exceptional synthesis method for getting similar morphological features that produced by high temperature hydrothermal process is considered a required task.

In the present work, the formation of nickel phosphate from its precursor salts via hydrothermal process based on simple reflux method will be reported. Hydrothermal process based on reflux -based route can handle those drawbacks since it is an efficient technique due to it is simple and costly effective. Moreover, we are going to study and evaluate the electrochemical oxidation of FAL on nickel phosphate modified glassy electrode GC/nano-NiPh. The material (nano-NiPh) will be characterized by FE-SEM, TEM, SAED and XRD. Electrochemical characterization and measurements for the GC/NiPh in blank (0.1 M NaOH) and in presence of FAL will be performed using cyclic voltammetry, chronoamperometry, open circuit potential and EIS measurements. Different kinetics and transport parameters will be estimated.

2. Experimental

2.1. Preparation of nickel phosphate

The chemicals of high purity (analytical grade) have been purchased from Sigma-Aldrich and Fisher. They have been used without further purification (as received). All solutions were prepared using deionized water. Nickel phosphate was synthesized using a hydrothermal process based on simple reflux method. The details of the hydrothermal process can be found in our previously published work [52]. However, here in, some details will be given briefly. A precipitate of nickel phosphate was mainly prepared from nickel nitrate ($Ni(NO_3)_2{\cdot}6H_2O$) and ammonium dibasic phosphate ($(NH_4)_2HPO_4$). Few drops of conc. nitric acid were added to dissolve the precipitate and to get a uniform homogenous solution. A 50 mL of 0.8 M urea solution was added to the homogenous mixture. Refluxing of the above solution was done at 90 °C with a uniform stirring for 15 h. The obtained suspension was left to cool to room temperature, filtered and washed several times with deionized water. Finally, the precipitate was left in an oven at 100 °C to dry for overnight to be ready for different characterizations.

Preparation of the catalyst ink of NiPh, for being anchored on the surface of glassy carbon electrode (GC), was prepared by adding the proper mass of the nano-NiPh powder (10 mg) in a test tube containing 2.5 mL isopropanol + 50 µL of Nafion solution (5% in water). The above mixture was sonicated for 30 min in an ice bath.

2.2. Fabrication of the electrode

Glassy carbon, GC (φ = 2 mm) is used here as the underlying substrate for nickel phosphate nanoparticles. It was cleaned by mechanical polishing with aqueous slurries of successively finer alumina powder (down to 0.06 µm), then washed thoroughly with deionized water and then with ethanol. Next, 50 µL of a freshly prepared nano-NiPh suspension (prepared as given above) was casted onto the thus cleaned GC electrode and left overnight for drying in air. The prepared loading level is 2.5 mg cm^{-2} (of the electrode surface area).

2.3. Measurements

A field emission scanning electron microscope, FE-SEM, (QUANTA FEG 250), high resolution transmission electron micrograph, TEM and X-ray diffraction, XRD (PANalytical, X'Pert PRO) operated with Cu target (λ = 1.54 Å) were used to identify the crystallographic structure of the nano-NiPh. XRD radiation generated at 40 kV and a current of 44 mA with a scan rate of 2°/min over a 2° range of 4–80°.

Electrochemical measurements were performed using Gamry potentiostat/galvanostat supported with Gamry electrochemical analysis technique. Electrochemical measurements were carried out in a conventional three-electrode cell. The counter electrode was made of a platinum coil. The reference electrode was Ag/AgCl/KCl (sat.) with a Luggin probe positioned near the electrode surface. The potential throughout the text is referred to the above reference electrode. The EIS measurements were carried out in the frequency range from 10 mHz to 100 kHz and using a signal of amplitude 5 mV peak-to-peak. The potential was kept constant (at 0.52 V in this work) for 500 s until

constant current (steady state conditions) and then the EIS was measured. The measurements were repeated to test the reproducibility of the results.

3. Results and discussion

3.1. Surface and electrochemical characterization

The surface morphology of the bare GC and the GC/NiPh material is illustrated by FE-SEM as shown in Fig. 1A and 1B, respectively. The microimage of the bare GC is featureless. The FE-SEM microimage for the GC/NiPh demonstrates that the NiPh particles are produced in one dimensional nanorods with average dimensions of (200 nm × 800 nm). Uniform distribution of the size and shape of the particles with apparent agglomeration are demonstrated. In Fig. 2A, the TEM image display a rod-like shape and nanoporous surface (see inset). The pore size can be estimated to be in the range of 20–30 nm. The SAED pattern of this sample is given in Fig. 2B. The bright dotes indicate a crystalline material which is consistent with the XRD pattern (*c.f.* Fig. 3). The chemical identity of the nano-NiPh powder can be determined from the XRD pattern as shown in Fig. 3. Table 1 shows the different peak positions and the corresponding 2θ value. According to the pattern and the data in Table 1, the composition of the material is found to be $Ni_3(PO_4)_2{\cdot}8H_2O$ with a monoclinic crystallographic form with the given characteristic peaks of the NiPh appear at 2θ values that are compatible with the standard spectrum (PDF. No. 33-0591) [53]. The XRD pattern demonstrates the sample was formed in a single phase structure. The average grain size D_{hkl} is estimated to be 51.0 nm for the NiPh prepared by the present experimental conditions. The above XRD pattern was confirmed by FT-IR absorption spectroscopy and the BET surface area was found to be 22.0 $m^2\,g^{-1}$ (see details in the supplementary document).

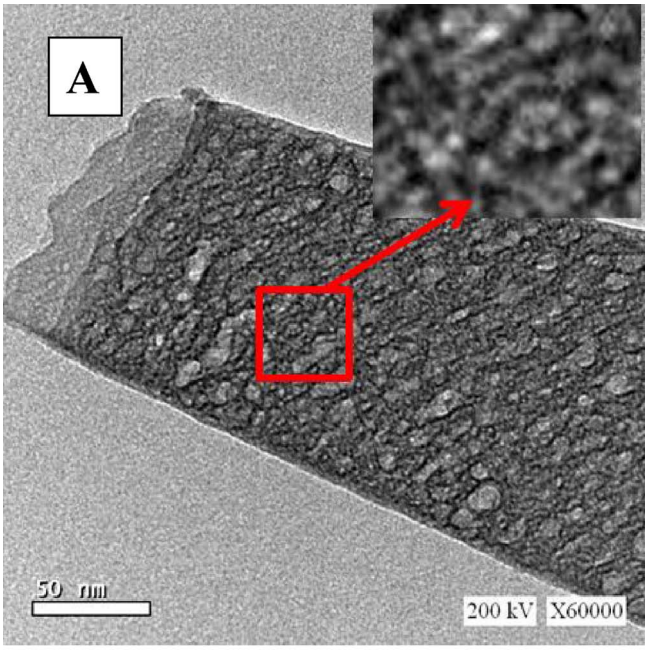

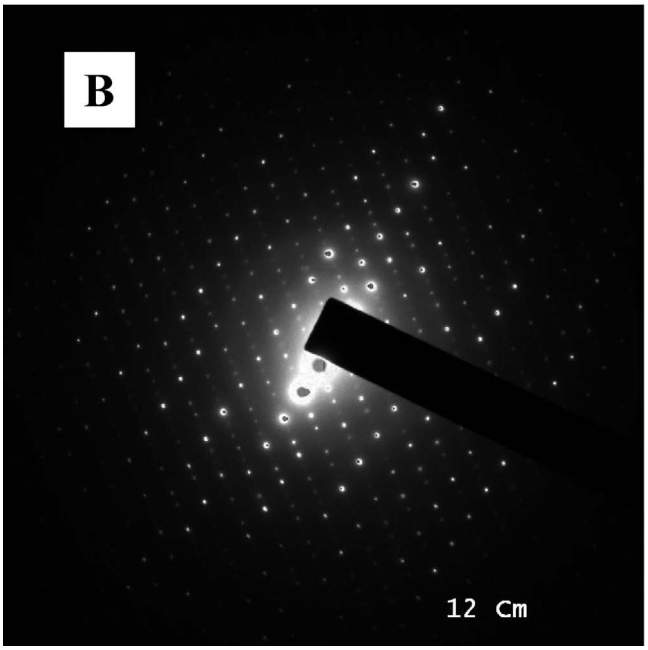

Fig. 2. (A) TEM image of the NiPh and (B) Selected-area electron diffraction (SAED) pattern.

Invasion of the OH^- ions from the alkali (0.1 M NaOH) was considered as a substantial approach in which the NiPh matrix can be enriched with Ni(II) and Ni(III) species (see Eq. (1)). In this study, potential cycling in the range from −0.1 to 0.75 V was done for 60 cycle. The consecutive CVs are represented in Fig. 4. Only 1st, 10th, 20th, 40th, 50th and 60th cycles are presented here for simplicity. At cycle number one, no significant peaks were emerged. By continuous potential cycling, the peaks of a redox couple were emerged and became obvious after the first ten cycles. The peak current of both the anodic and cathodic sweeps increases with the number of cycles up to the 50th cycle after which there is no significant increase of the current up to cycle number ~60. The following reaction occurs during the activation process [52,54];

$$Ni_3(PO_4)_2 + 3OH^- \rightarrow Ni_3(OH)_3(PO_4)_2 + 3e \quad (1)$$

Note that nickel is divalent (Ni(II)) in the synthesized material ($Ni_3(PO_4)_2$) and trivalent (Ni(III)) in $Ni_3(OH)_3(PO_4)_2$. This implies a redox couple built inside the NiPh matrix. In this study, Ni(II) and Ni(III) will be assigned for the divalent nickel (NiPh(II)) and trivalent nickel NiPh(III), respectively. Accordingly, the redox couple may be written as Ni(II)/Ni(III). Immersion of the GC/nano-NiPh in the alkali (0.1 M NaOH) does not produce such activation (i.e., not producing Ni redox species) and consequently the above potential cycling in 0.1 M NaOH is essential for such activation process. Fig. 5 shows the open circuit potential, E_{oc} of the GC/nano-NiPh before (curve a) and after (curve b) the above activation process. It is obvious that E_{oc} before (curve a) has almost a constant value approaching −0.03 V. However, the value after activation (curve b), increases in the positive direction and rapidly reaches to a more positive value and stabilized at ~0.06 V.

For further investigation of the GC/nano-NiPh, an electrochemical impedance (EIS) was measured. Fig. 6 depicts Nyquist plots in blank 0.1 M NaOH before (plot a) and after the above activation process (plot b). The latter (plot b) demonstrates a depressed semicircle while the former (curve a, before activation) exhibit tilted straight line characteristics of low conductivity electrode material [55]. Fitting of the impedance data in Fig. 6 is performed by replacing the capacitor, *C* with constant phase element, *CPE* in the equivalent circuit (Q_{dl} in the inset of Fig. 6). The use of *CPE* in modeling is to account for frequency dispersion behavior corresponding to some physicochemical processes

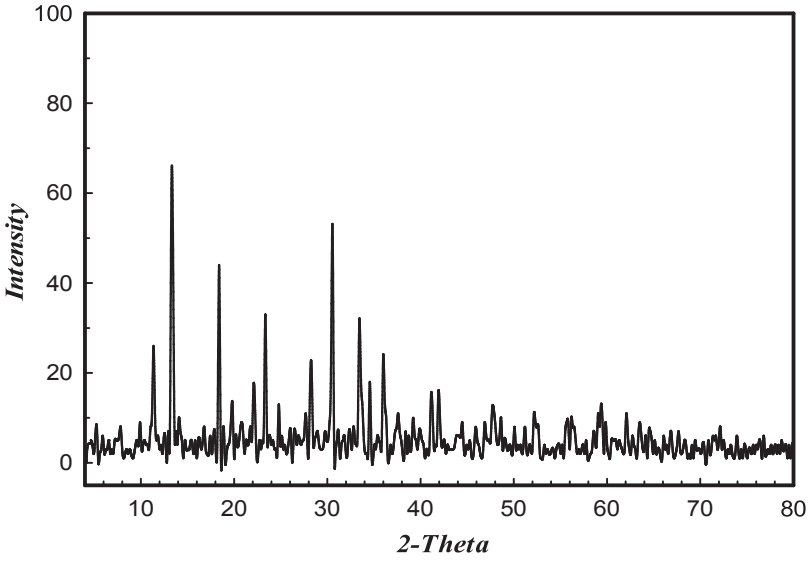

Fig. 3. XRD pattern of the NiPh.

Table 1
XRD pattern data.

Angle 2θ	d value Å	Index
11.324	7.80784	(110)
13.351	6.62652	(020)
18.408	4.81598	(200)
19.776	4.48582	(130)
22.149	4.01028	(−101)
23.368	3.80374	(101)
28.233	3.15829	(031)
30.512	2.92742	(−301)
33.426	2.67855	(−321)
33.662	2.66033	(330)
34.537	2.59494	(141)
35.99	2.49342	(301)
37.61	2.38963	(−112)
39.454	2.28213	(051)
41.18	2.19034	(−341)
41.95	2.1519	(−251)
44.402	2.03861	(351)
48.567	1.87307	(132)
55.594	1.6518	(080)
59.339	1.55617	(501)

such as surface inhomogeneity resulting from surface roughness, distribution of the active sites, dislocations, impurities and possible adsorption process [56,57]. The charge transfer resistance, R_{ct} of the GC/nano-NiPh was found to be 9.90 and 2.35 kohm cm^2 before and after the activation process, respectively. This implies that the conductivity of the NiPh matrix increases with the activation process due to enrichment of the matrix with the redox species (Ni(II) and Ni(III)) and hence higher charge transfer rate is obtained.

After the above activation process, the GC/nano-NiPh was characterized by measuring cyclic voltammetry responses (CVs) at different scan rates (from 5 to 1200 mV s^{-1}) in blank 0.1 M NaOH as depicted in Fig. 7A. The CVs reveal one anodic peak and one cathodic peak in the potential range of ~0.42–0.75 V. This is assigned for the redox transform Ni(II)/Ni(III) as described before. Both anodic peak current, I_{pa} and cathodic peak current, I_{pc} increase with the scan rate, ν. Also, the peak separation of the anodic and cathodic peak potentials increases with the scan rate. The peak current of the cathodic sweep is less than the anodic peak current. The above findings are characterized of quasi-reversible process. Fig. 7B represents plots of I_{pa} and I_{pc} with the scan rate, ν. The plots show straight lines in both the anodic and cathodic scans. This indicates a surface-confined redox couple [58].

In order to determine the charge transfer coefficient, α of the above redox transformation, a plot of the peak potential, E_p in the anodic (E_{pa}) and cathodic (E_{pc}) sweeps with the natural logarithm of the scan rate is given (see Fig. 7C). A linear relation was obtained at $\Delta E_p > 200/n$ mV where n is the number of exchange electrons. This is in accordance with Lavrion approach according to the following equations [27,59];

$$E_{pa} = E^o + \frac{RT}{(1-\alpha)nF} \times \ln\left[\frac{(1-\alpha)nF\nu}{RTk_s}\right] \quad (2)$$

$$E_{pa} = E^o + \frac{RT}{\alpha nF} \times \ln\left[\frac{\alpha nF\nu}{RTk_s}\right] \quad (3)$$

$$\ln k_s = \alpha \ln(1-\alpha) + (1-\alpha)\ln\alpha - \ln\left(\frac{RT}{nF\nu}\right) - \left(\frac{\alpha(1-\alpha)\, nF\Delta E_p}{RT}\right) \quad (4)$$

Where E^o is the standard electrode potential and R, T and F have their usual meanings, k_s is the charge transfer rate constant and ν is the potential scan rate in V s^{-1}. Using the slope of the relation between E_p and ln ν, the value of the anodic charge transfer coefficient, α was found to be 0.75. This value may be explained in the light of the different limiting step in the cathodic and anodic transforms [60]. The mean value of the charge-transfer rate constant, k_s over the used scan rate range is calculated to be 0.063 s^{-1}. This value can be compared with the literature values [24,27].

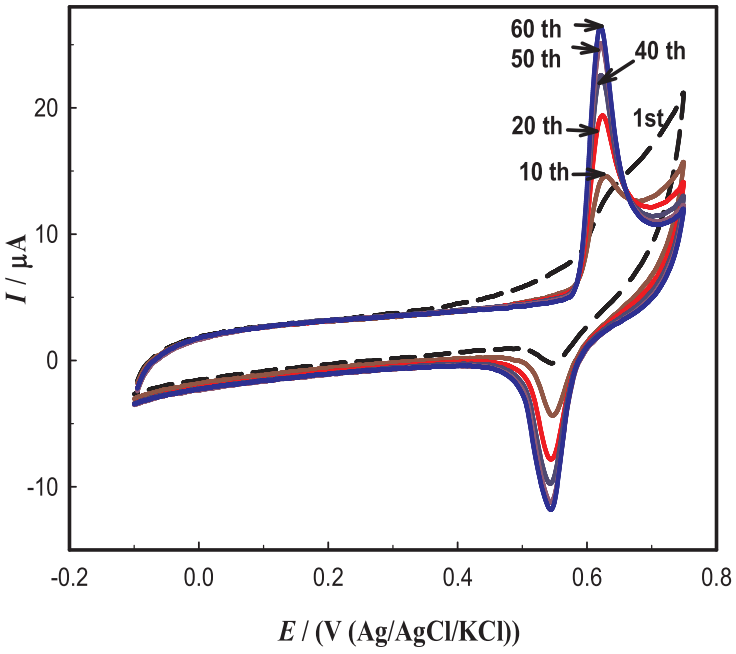

Fig. 4. Activation of GC/nano-NiPh by continuous potential cycling at scan rate of 100 mV s^{-1} for 60 cycles. Representative cycles are only shown here.

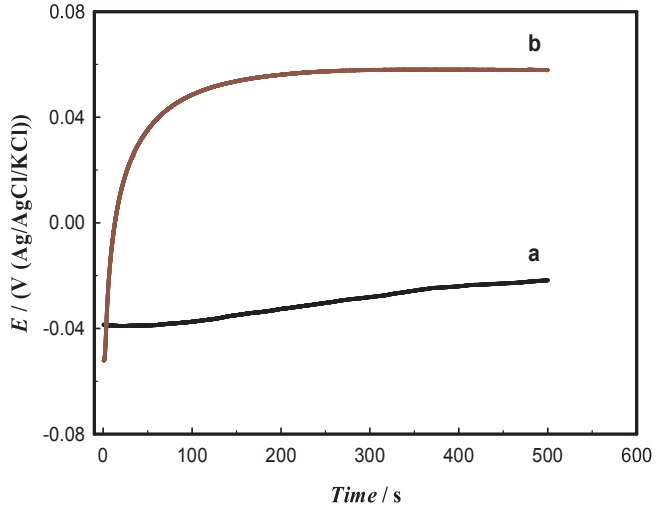

Fig. 5. Open circuit potential, E_{oc}-time curves of GC/nano-NiPh before (a) and after (b) the activation process presented in Fig. 4.

3.2. Electrooxidation of formaldehyde

The electrochemical oxidation of FAL on the GC/nano-NiPh will be assessed in this section by collecting CV responses at different conditions. Fig. 8 shows CV responses of GC (a, b) and GC/nano-NiPh (c, d) in blank 0.1 M NaOH (a, c), and in 0.1 M NaOH containing 0.005 M FAL (b, d) at scan rate of 20 mV s^{-1}. The GC electrode does not show any significant peaks in presence of the FAL and hence it can be concluded that GC is not active for FAL oxidation. Curve (c) demonstrates redox peaks of the Ni(II)/Ni(III) as seen before in Fig. 7A. In the presence of FAL (curve d), a dramatic high anodic peak reveals. Its peak current is much higher than that of the blank (in absence of FAL, curve (c)). This is attributed to the electrochemical oxidation of FAL on the GC/nano-NiPh electrode. The peak potential of the FAL oxidation is ~0.7 V which is higher enough than the peak potential of the NiPh(II)/NiPh (III) redox couple. It refers to the fact that the FAL oxidation starts after considerable formation of the Ni(III) species. Also, the cathodic peak of the Ni(III) → Ni(II) is diminished as Ni(III) was consumed by the FAL indicating the electrocatalytic nature of the process. One further note is; at the backward sweep (see arrows in the figure) in presence of FAL another anodic peak is revealed which is assigned for further oxidation of the FAL but with lower peak current than that obtained in the forward scan. During the forward sweep, the Ni(II) species are converted to Ni(III) species and in turn FAL reacts with the Ni(III) species converting them to Ni(II). During the backward scan, the recovery of the active sites of Ni(III) species was not complete and hence the peak current of FAL oxidation in the backward direction is less than that of the forward direction.

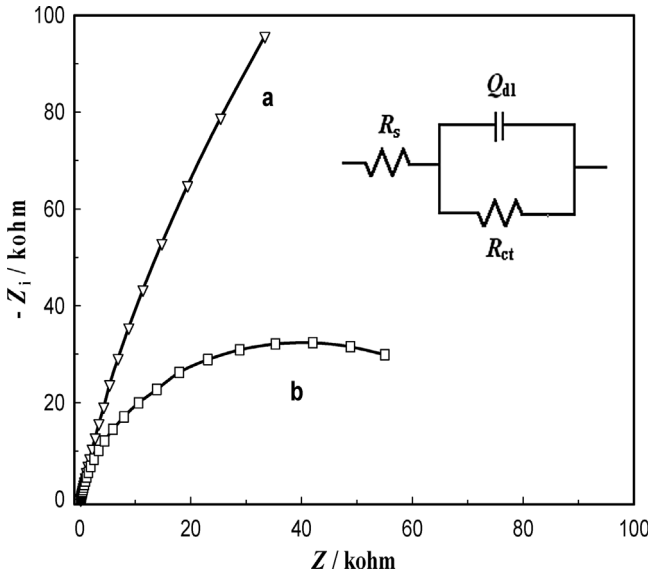

Fig. 6. Nyquist Plots of GC/nano-NiPh before (a) and after (b) the activation process presented in Fig. 4. The inset shows the equivalent circuit.

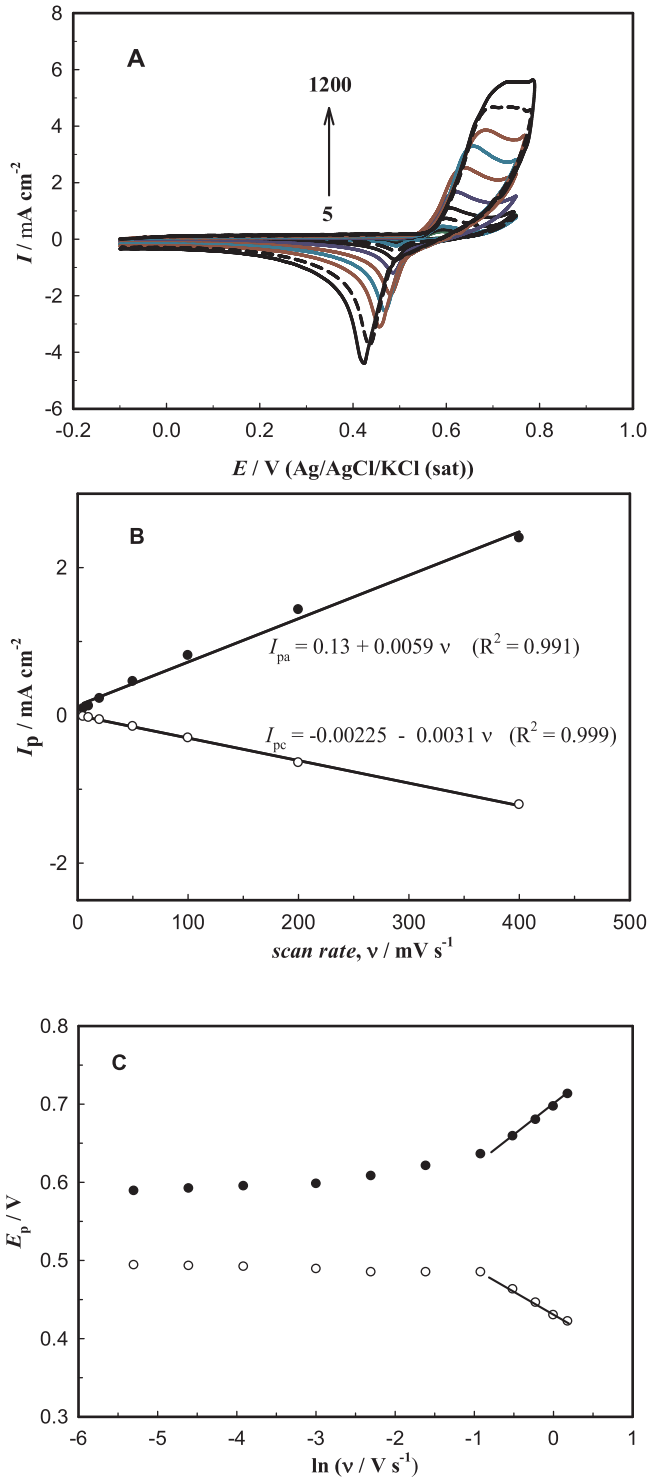

Fig. 7. (A) CV responses of GC/nano-NiPh in 0.1 M NaOH at different scan rates. From inner: 5, 10, 20, 50, 100, 200, 400, 600, 800, 1000, 1200 mV s^{-1}. (B) Relation between I_p and the scan rate. (C) Relation between E_p and natural logarithm of the scan rate, ν.

Fig. 9A shows CV responses of the GC/nano-NiPh in 0.1 M NaOH containing 0.005 M FAL at different scan rates. As the scan rate increases, the anodic peak current of FAL oxidation increases. Also, the residual cathodic peak assigned for the reduction of the remaining Ni (III) species to Ni(II) increases with the scan rate. This may point to the fact that the remained [Ni(III)] increases with increasing the scan rate due to lower consumption of the Ni(III) species at higher scan rates. The above CVs data can be investigated by plotting the peak current, I_p with the square root of the scan rate, $\nu^{0.5}$ (Fig. 9B). The data was obtained from Fig. 9A. A straight line is obtained (R^2 = 0.997) which is in accordance with the Randles-Sevcik equation for completely irreversible diffusion-controlled process [61]. It is given by the following equation;

$$I_p = 0.4961x\, n\, F\left(\frac{\alpha n_a F\, D_o}{RT}\right)^{0.5} A\, C\, \nu^{0.5} \quad (5)$$

Where A is the surface area of the working electrode, D_o is the diffusion coefficient of formaldehyde, n is the total number of electrons (n = 1) [24], C is the bulk concentration of formaldehyde and ν is the potential scan rate. Also, α is the charge transfer coefficient, n_a is the number of electrons in the rate-determining step, F is the Faraday's constant, R is the gas constant and T is the absolute temperature. The value of αn_a can be determined by using the following equation [62];

$$|E_p - E_{p/2}| = \frac{1.857\, RT}{\alpha n_a\, F} \quad (6)$$

Where E_p and $E_{p/2}$ are the peak potential and the potential at half peak current, respectively. The parameters R, T and F have their usual meanings. The data in Fig. 9A was used to calculate the parameter αn_a at different scan rates. The average value was found to be 0.495. Note that this value is less than that obtained in blank which may point to some kinetic limitations in presence of the FAL due to possible poisoning of the electrode surface with the electrochemical oxidation products. The diffusion coefficient, D_o was determined from Eq. (5) to be 1.4 × 10^{-4} cm^2 s^{-1} by using the slope of the straight line in Fig. 9B and the value of αn_a. This value is closer to those found in literatures [23]. Fig. 9C depicts a plot of $I_p.\nu^{-0.5}$ with the scan rate. It represents the characteristics features of typical catalyst regeneration mechanism. This can be suggested in the light of the catalyst regeneration mechanism during the electrocatalytic oxidation of FAL on the GC/nano-NiPh [63].

The stability of the electrocatalyst is critical in evaluating the performance of the electrocatalyst for oxidation of organic molecules (FAL in our case). This can be done either by measuring transient current-time relations or potential cycling during the electrochemical oxidation of the organic molecule. Fig. 10A depicts consecutive CV responses

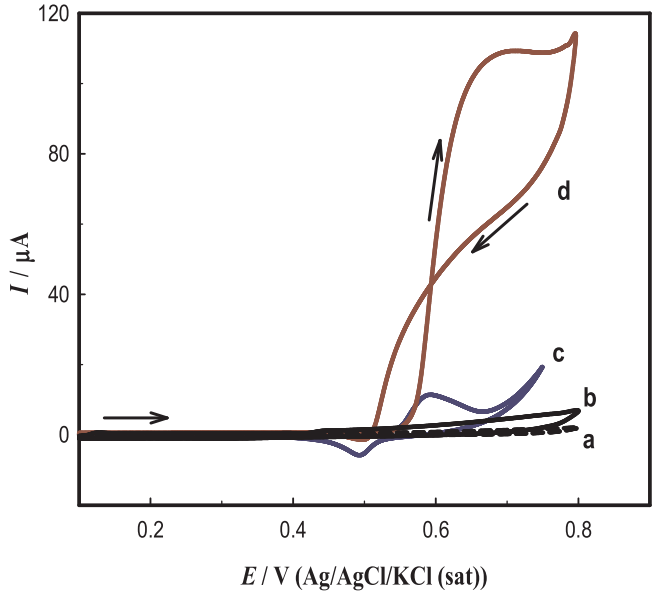

Fig. 8. CV responses of GC (a, b) and GC/nano-NiPh (c, d) in blank 0.1 M NaOH (a, c) and in 0.1 M NaOH containing 0.005 M FAL (b, d), at scan rate of 20 mV s^{-1}.

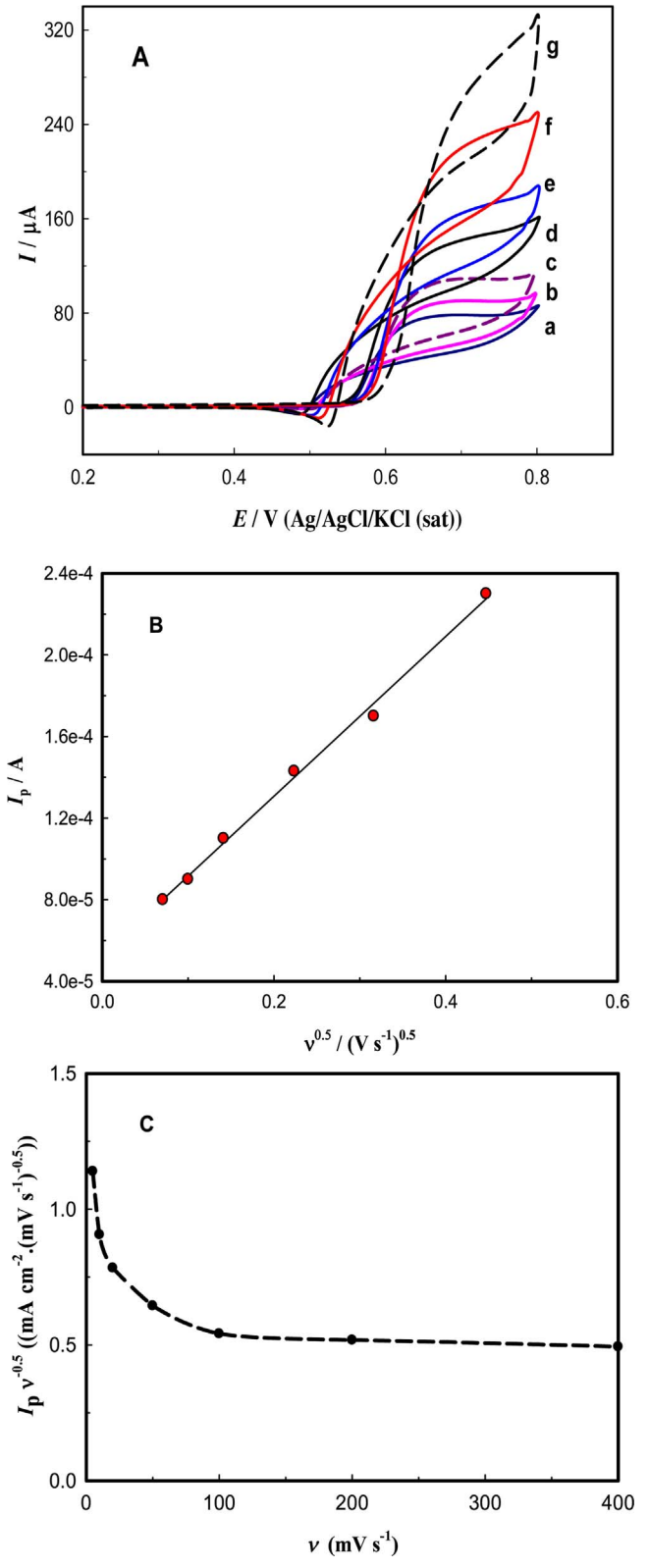

Fig. 9. (A) CV responses of GC/nano-NiPh in 0.1 M NaOH at different potential scan rates, (a) 5, (b) 10, (c) 20, (d) 50, (e) 100, (f) 200 and (g) 400 mV s^{-1}. (B) Plot I_p of FAL electrochemical oxidation and the square of the scan rate, $\nu^{0.5}$. (C) Relation between I_p $\nu^{-0.5}$ with the scan rate.

obtained for FAL electrochemical oxidation on the GC/nano-NiPh in 0.1 M NaOH containing 0.005 M FAL and scan rate of 100 mV s^{-1}. The number of potential cycles was 50 cycles. The CVs both in the forward scan and backward scan reveal higher currents at the first five cycles before it tends to decrease gradually with the number of cycles (number of cycles > 5) until getting similar overlaid CVs. Fig. 10B depicts the relations between the peak current, I_p of the forward scan (curve a) and that of the backward scan (curve b) with the number of cycles. Initially, I_p increases due to possible activation of the electrode due to re-generation of the active sites on the electrode surface. After cycle number six, the I_p starts to decrease due to the accumulation of the oxidation products on the GC/nano-NiPh surface that causes some extent of surface poisoning and consequently the current decreases to some extent. After the peak number 36, the current keeps constant values due to the trade-off between the regeneration of the active sites (causes increase in current) and the surface poisoning (causes decrease in current) and hence the current is stabilized at these values.

Based on the above results, we may propose a mechanism for the electrooxidation of FAL on the GC/nano-NiPh as given in Fig. 11. In aqueous NaOH solution, formaldehyde is completely hydrated and

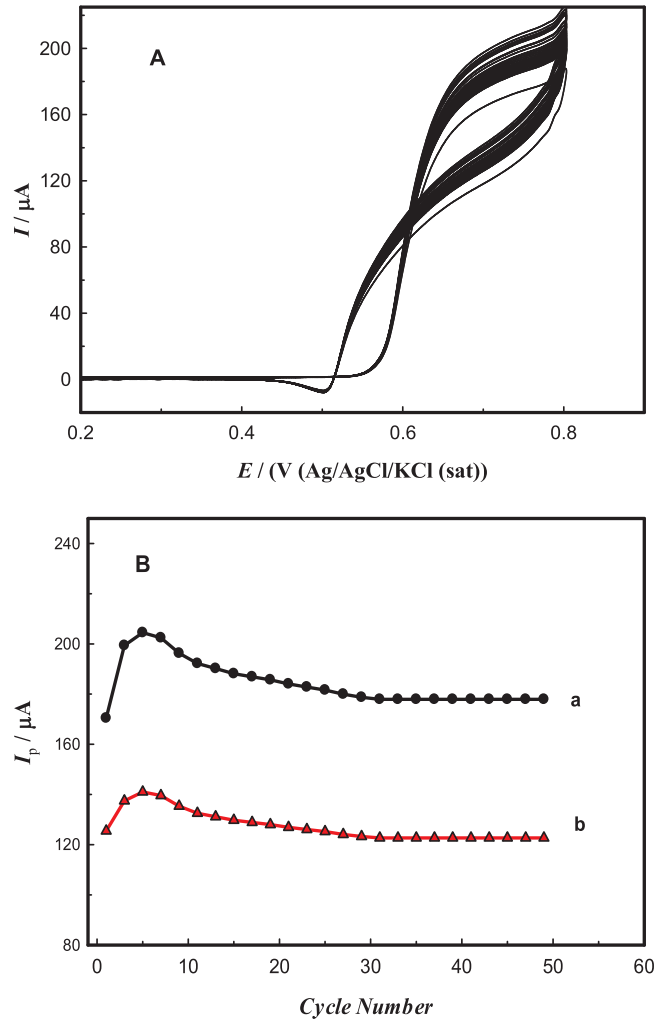

Fig. 10. (A) Consecutive CV responses of GC/nano-NiPh in 0.1 M NaOH containing 0.005 M FAL. (B) I_p with the cycle number for the forward scan (a) and backward scan (b).

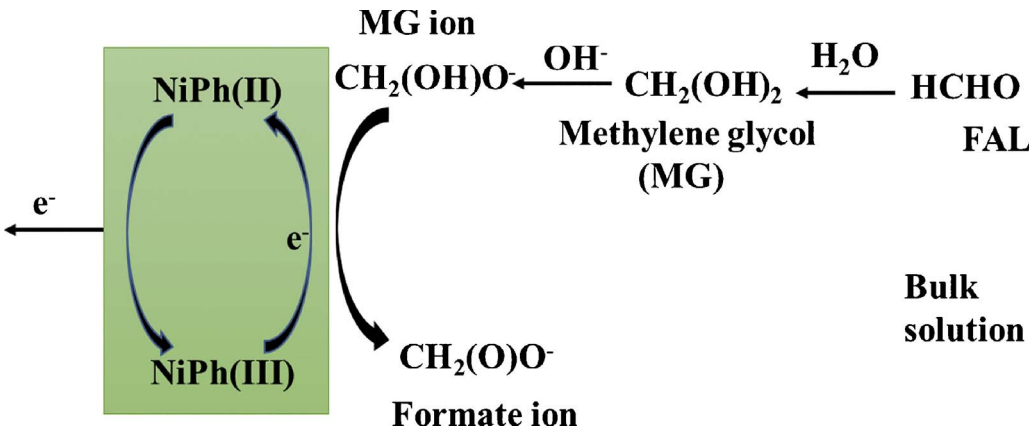

Fig. 11. Schematic of the mechanism of the FAL electrocatalytic oxidation.

converted to methylene glycol $CH_2(OH)_2$ with an equilibrium constant value of 1.0×10^3 [21]. Due to its pK_a of ca. 12.8, the methylene glycol exists predominantly in its ionized form ($CH_2(OH)O^-$) in 0.1 M NaOH. When $CH_2(OH)O^-$ diffuses from the bulk solution to the electrode surface, the methylene glycol ion is quickly oxidized to $CHOO^-$ by the Ni(III) species on the electrode [21]. The electrocatalytic oxidation mechanism of HCHO at the GC/nano-NiPh surface may be described by the followings:

$$3CH_2O + 3H_2O \leftrightarrows 3CH_2(OH)_2 \; K_{eq} = 2.28 \times 10^3 \quad (7)$$

$$3CH_2(OH)_2 + 3OH^- \leftrightarrows 3CH_2(OH)O^- + 3H_2O \quad (8)$$

$$Ni(II) + 3OH^- \leftrightarrows Ni(III)(OH)_3 + 3e^- \quad (9)$$

$$3CH_2(OH)O^- + Ni(III)(OH)_3 \rightarrow Ni(II) + 3CH2(O)O^- + 3H_2O \quad (10)$$

The sum of the above equations could be;

$$3CH_2O + 6OH^- \rightarrow 3CH_2(O)O^- + 3e^- \quad (11)$$

For simplicity we referred to NiPh(II) and NiPh(III) as Ni(II) and Ni (III), respectively (see Eq. (1)). The electrocatalytic mechanism is in accordance with the results in Fig. 8. According to the present results the GC/nano-NiPh demonstrated enhancement electrochemical oxidation of FAL. According to Eq. (1) the redox couple Ni(II)/Ni(III) is embedded in the phosphate matrix which enhances the stability of the above redox couple as shown in Fig. 10. This is in accordance with some literatures which used NiPh for electrocatalytic reactions [64]. The electrocatalytic properties of the GC/nano-NiPh may be also attributed to the high adsorbability of the phosphate ions, PO_4^{3-} to the small organic compound [65] which are advantages for using NiPh as an electrocatalyst.

Further investigation of the electrocatalytic oxidation of FAL can be done by chronoamperometry measurements. Cottrell equation is given by;

$$I = n\,FA\;D^{0.5}C\,\pi^{-0.5}\,t^{-0.5} \quad (10)$$

Where n is the number of electrons needed for the conversion of one molecule of FAL and the t is the time in seconds (s) and the rest of parameters has the same meanings as in Eq. (5). Fig. 12A shows the chronoamperometric curves of FAL oxidation on the GC/nano-NiPh in 0.1 M KOH containing different concentrations of FAL. The onset shows a plots of the current, I with $t^{-0.5}$. The plots reveal straight lines ($R^2 = 0.995$). Using the slopes of these lines, the diffusion coefficients were estimated to be 1.97×10^{-4}, 1.1×10^{-4} and 5.5×10^{-5} $cm^2\,s^{-1}$ in 0.0025, 0.004 and 0.01 M FAL, respectively with average value of 1.2×10^{-4} $cm^2\,s^{-1}$. This value is comparable with the value calculated from Eq. (5). Fig. 12B shows chronoamperometric curves of the GC/nano-NiPh in blank (a) (0.1 M NaOH) and in 0.1 M NaOH containing 0.005 M FAL (b). The catalytic rate constant, k_{cat} of the electrocatalytic oxidation of FAL can be calculated from the following equation [60];

$$\frac{I_{cat}}{I_L} = \pi^{0.5}(k_{cat}C^o t)^{0.5} \quad (12)$$

Where I_{cat} and I_L is the current in presence and absence of FAL, respectively, and C^o is the [FAL] in mol cm^{-3}. The inset of Fig. 12B shows a plot of I_{cat}/I_L with $t^{0.5}$. From the slope of the obtained straight line, the value of k_{cat} was found to be 4.1×10^6 $cm^3\,mol^{-1}\,s^{-1}$. Table 2 lists comparison of some parameters (including the k_{cat} value) found here in this study with their corresponding values in literatures. The chronocoulometry curves are shown in Fig. 12C in absence (a) and presence (b) of 0.005 M FAL. The results point to the higher charge consumed by FAL during its electrocatalytic oxidation. Comparison of the various parameters obtained here in our study with the literatures can be given to further evaluate the present electrode, GC/nano-NiPh. Table 2 lists the values of the catalytic rate constant, k_{cat}, peak potential, E_{pa} and the current density of the FAL electrochemical oxidation. As can be seen from the Table, the obtained values here in this work are better than in many cases and comparable with others. Being cost-effective, the reflux–based hydrothermal process used here in this work may add some value to the present work.

4. Conclusions

Nickel phosphate (NiPh) was synthesized using simple hydrothermal process. The NiPh particles revealed nanoporous structure. The material was characterized by different techniques including surface and structural (FE-SEM, XRD and TEM) and electrochemical techniques (CV, EIS and chronoamperometric). GC/nano-NiPh showed enhanced electrocatalytic activity towards electrochemical oxidation of formaldehyde from alkaline solution. Some important kinetic and transport parameters of the above process were extracted and compared with literatures. The stability and the performance of the GC/nano-NiPh was evaluated at the prevailed experimental conditions.

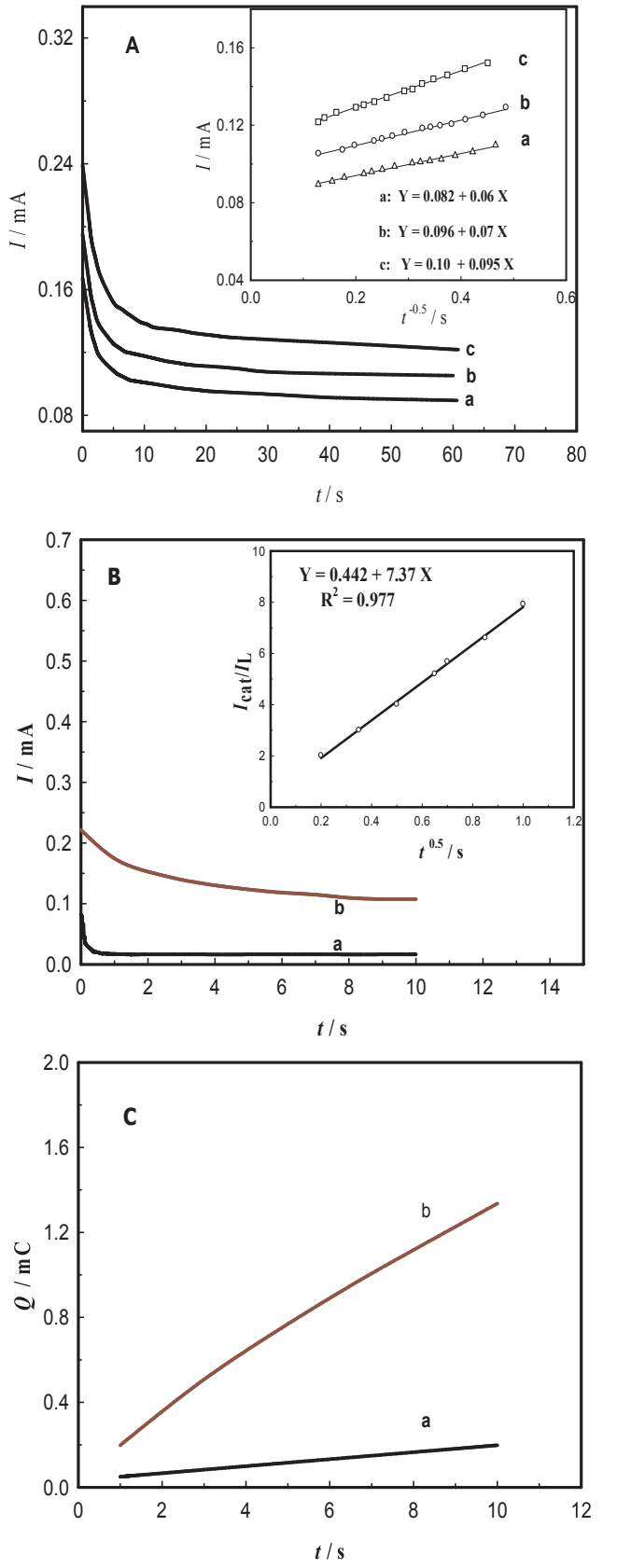

Fig. 12. (A) Chronoamperometric curves and the inset shows the I-$t^{-0.5}$ plots for FAL electrochemical oxidation in 0.1 M NaOH containing different FAL concentrations: (a) 0.0025, (b) 0.004 and (c) 0.01 M. (B) Chronoamperometric curves for GC/nano-NiPh in blank 0.1 M NaOH (a) and in 0.1 M NaOH containing 0.005 M FAL (b). The inset shows the relation between I_{cat}/I_L and $t^{0.5}$. (C) Chronocoulometry curves with the same labels and conditions in Panel A.

Table 2
Comparison of the catalytic rate constant, k_{cat}, peak potential, E_p and current density of the FAL electrochemical oxidation with literatures. The [FAL] = 0.005 M at scan rate of 20 mV s^{-1}.

Ref	Electrode	k_{cat}/cm^3 mol^{-1} s^{-1}	E_p/V (Ag/AgCl/KCl)	I/mA cm^{-2}
[27]	Ni-CoVSB-5/CPE	1.8×10^5	0.73	2.29
[22]	Ni/IL/CPE	1.6×10^6	0.53	2.20
[23]	Ni/P(NMA)/MCPE	9.0×10^4	0.58	3.30
[66]	Ni/ANACPE	7.5×10^4	0.7	1.42
[24]	Ni-CHIT/CPE	2.0×10^5	0.51	4.16
[67]	P-1,5-DAN/MCPE	2.0×10^6	0.58	0.88
[68]	Ni(OH)$_2$-X/CPE	6.1×10^6	0.60	3.54
[69]	Ni/P-CPE	1.7×10^4	0.62	4.80
This study	GC/nano-NiPh	4.0×10^6	0.70	3.50

Appendix A. Supplementary data

Supplementary data associated with this article can be found, in the online version, at http://dx.doi.org/10.1016/j.apcatb.2017.11.031.

References

[1] X. Yu, P.G. Pickup, J. Power Sources 182 (2008) 124–132.
[2] R. Ojani, J.-Bakhsh Raoof, Y. Ahmady-Khanghah, S. Safshekan, Int. J. Hydrogen Energy 38 (2013) 5457–5463.
[3] H.M. Villullas, F.I. Mattos-Costa, P.A.P. Nascente, L.O.S. Bulhoes, Electrochim. Acta 49 (2004) 3909–3916.
[4] R. Ojani, J.B. Raoof, S.R.H. Zavvarmahalleh, J. Solid State Electrochem. 13 (2009) 1605–1611.
[5] S. Park, Y. Xie, M.J. Weaver, Langmuir 18 (2002) 5792–5798.
[6] Y. Yu, T. Wang, Y. Fu, W. Su, J. Hu, Int. J. Hydrogen Energy 39 (2014) 17617–17621.
[7] R.H. Tammam, M.M. Saleh, J. Power Sources 246 (2014) 178–183.
[8] Z.H. Zhang, X.C. Zhou, C.P. Liu, W. Xing, Electrochem. Commun. 10 (2008) 131–135.
[9] M.J. Croissant, T. Napporn, J.-M. Léger, C. Lamy, Electrochim. Acta 43 (1998) 2447–2457.
[10] L.A. Hutton, M. Vidotti, A.N. Patel, M.E. Newton, P.R. Unwin, J.V. Macpherson, J. Phys. Chem. C 115 (2011) 1649–1659.
[11] M. Vidotti, S.I.C. de Torresi, L.T. Kubota, Sens. Actuator B 135 (2008) 245–249.
[12] Q.F. Yi, J.J. Zhang, W. Huang, X.P. Liu, Catal. Commun. 8 (2007) 1017–1022.
[13] I. Danaee, M. Jafarian, A. Mirzapoor, F. Gobal, M.G. Mahjani, Electrochim. Acta 55 (2010) 2093–2100.
[14] A. Arvinte, A.C. Westermann, A.M. Sesay, V. Virtanen, Sens. Actuator B 150 (2010) 756–763.
[15] A. Kapałka, A. Cally, S. Neodo, C. Comninellis, M. Wächter, K.M. Udert, Electrochem. Commun. 12 (2010) 18–21.
[16] J. Yang, J. Tan, F. Yang, X. Li, X. Liu, D. Ma, Electrochem. Commun. 23 (2012) 13–16.
[17] A. Samadi-Maybodi, Seyed Karim Hassani Nejad-Darzi, M. Ganjali, H. Ilkhani, J. Solid State Electrochem. 17 (2013) 2043–2048.
[18] D. Yang, Q. Yu, L. Gao, L. Mao, J.H. Yang, Appl. Surf. Sci. 416 (2017) 503–510.
[19] J.B. Raoof, M. A.Karimi, S.R. Hosseini, S. Mangelizade, Int. J. Hydrogen Energy 36 (2011) 1381–13287.
[20] Y. Yu, W. Su, M. Yuan, Y. Fu, J. Hu, J. Power Sources 286 (2015) 130–135.
[21] A. Ciszewski, G. Milczarek, J. Electroanal. Chem. 469 (1999) 18–26.
[22] R. Ojani, J.B. Raoof, S. Safshekan, J. Appl. Electrochem. 42 (2012) 81–87.
[23] J.B. Raoof, A. Omrani, R. Ojani, F. Monfared, J. Electroanal. Chem. 633 (2009) 153–158.
[24] S.K. Hassaninejad–Darzi, J. Electroceram. 33 (2014) 252–263.
[25] C. Zhao, M. Li, K. Jiao, J. Anal. Chem. 61 (2006) 1204–1208.
[26] J. Zhang, L. Shangguan, S. Shuang, C. Dong, Russ. J. Electrochem. 49 (2013) 888–894.
[27] S.K. Hassaninejad-Darzi1, M. Rahimnejad, M.G. Esfidvajani, Fuel Cells 16 (2016) 89–99.
[28] O.A. Rusu, W.F. Hoelderich, H. Wyart, M. Ibert, Appl. Catal. B: Environ. 176–177 (2015) 139–149.
[29] E. Kim, D. Son, T.G. Kim, J. Cho, B. Park, K.S. Ryu, S.H. Chang, Angew. Chem. Int. Ed. 43 (2004) 5987–5990.
[30] M.N. Timofeeva, Z. Hasan, A.Yu. Orlov, V.N. Panchenko, Y.A. Chesalov, I.E. Soshnikov, S.H. Jhung, Appl. Catal. B: Environ. 107 (2011) 197–204.
[31] M.N. Timofeeva, Zubair Hasan, V.N. Panchenko, I.P. Prosvirin, Sung Hwa Jhung, J. Mol. Catal. A: Chem. 363–364 (2012) 328–334.
[32] Mohamed M. Saleh, A.H. Touny, M.A. Al-Omair, M.M. Saleh, Bio-Med. Mater. Eng. 27 (2016) 87–99.

[33] J. Sánchez-Enríquez, J. Reyes-Gasga, Obtaining $Ca(H_2PO_4)_2$ H_2O, Ultrason. Sonochem. 20 (2013) 948–954.
[34] M.P. Ginebra, T. Traykova, J.A. Planell, J. Control Release 113 (2006) 102–110.
[35] A.A. Ahmed, A.A. Ali, D.A.R. Mahmoud, A.M. El-Fiqi, Solid State Sci. 13 (2011) 981–992.
[36] L. Cheng, M.D. Weir, H.K. Xu, J.M. Antonuccie, A.M. Kraigsleye, N.J. Line, S. Lin-Gibsone, X. Zhou, Dent. Mater. 28 (5) (2012) 561–572.
[37] A. Yamada, S.C. Chung, K. Hinokuma, J. Electrochem. Soc. 148 (2001) (2001) A224–A229.
[38] K. Zaghib, K. Striebel, A. Guerfi, J. Shim, M. Armand, M. Gauthier, Electrochim. Acta 50 (2004) 263–270.
[39] X. Zhao, B.M. Sanchez, P.J. Dobson, P.S. Grant, Nanoscale 3 (2011) 839–855.
[40] X. Peng, L. Peng, C. Wu, Y. Xie, Chem. Soc. Rev. 43 (2014) 3303–3323.
[41] S.H. Jhung, Jin-Ho Lee, A.K. Cheetham, Gérard Férey, Jong-San Chang, J. Catal. 239 (2006) 97–104.
[42] Y. Zhan, M. Lu, S. Yang, C. Xu, Z. Liu, J. Yang Lee, ChemCatChem 8 (2016) 372–379.
[43] Y. Liu, L. Zhang, Z. Shi, H. Yuan, W. Pang, J. Solid State Chem. 158 (2001) 68–73.
[44] X. Wang, Q. Gao, C. Wu, J. Hu, M. Ruan, Materials 85 (2005) 355–364.
[45] S. Jhung, J. Yoon, J. Hwang, A. Cheetham, J. Chang, Chem. Mater. 17 (2005) 4455–4460.
[46] H. Onoda, K. Asai, A. Takenaka, J. Ceram. Process. Res. 12 (4) (2011) 439–442.
[47] H. Onoda, T. Ohta, J. Tamaki, K. Kojima, H. Nariai, Mater. Chem. Phys. 96 (2006) 163–169.
[48] J. Yu, A. Wang, J. Tan, X. Li, J. Bokhoven, Mater. Chem. 18 (2008) 3601–3607.
[49] H. Wu, Y. Gaob, H. Li, Cryst. Eng. Comm. 12 (2010) 3607–3611.
[50] E. Muthuswamy, G.H. Layan Savithra, S.L. Brock, ACS Nano 5 (2011) 2402–2411.
[51] H. Yin, F. Liu, X. Chen, X. Feng, W. Tan, G. Qiu, Microporous Mesoporous Mater. 153 (2012) 115–123.
[52] M.A. Al-Omair, A.H. Touny, M.M. Saleh, J. Power Sources 342 (2017) 1032–1039.
[53] National Bureau of Standards Monograph 25, Section 19—Data for 51 Substances Natl. Bur. Stand. (U.S.), Monograph. 25-Sec. 19, 118 pages (Dec. 1982), CODEN: NBSMA6.
[54] Y. Zhan, M. Lu, S. Yang, Z. Liu, J. Yang Lee, ChemElectroChem 3 (2016) 615–621.
[55] G. Barral, S. Maximovitch, F. Njanjo-Eyoke, Electrochim. Acta 41 (1996) 1305–1311.
[56] R.H. Tammam, A.M. Fekry, M.M. Saleh, Int. J. Hydrogen Energy 40 (2015) 275–283.
[57] P. Singh, E.E. Ebenso, L.O. Olasunkanmi, I.B. Obot, M.A. Quraishi, J. Phys. Chem. C 120 (6) (2016) 3408–3419.
[58] A.S. Danial, M.I. Awad, F.A. Al-Odail, M.M. Saleh, J. Mol. Liq. 225 (2017) 919–925.
[59] E. Laviron, J. Electroanal, Chem. Int. Electrochem. 101 (1979) 19–28.
[60] H. Luo, Z. Shi, N. Li, Z. Gu, Q. Zhuang, Anal. Chem. 73 (2001) 915–920.
[61] A.J. Bard, L.R. Faulkner, Electrochemical Methods: Fundamentals and Applications, Wiley, New York, 1980.
[62] C.O. Laoire, S. Mukerjee, K.M. Abraham, H. Avenue, E.J. Plichta, M.A. Hendrickson, J. Phys. Chem. C 113 (46) (2009) 20127–20134.
[63] S.M. El-Refaei, B.E. El-Anadouli, M.I. Awad, Mahmoud M. Saleh, Electrochim. Acta 92 (2013) 460–467.
[64] M.A. Al-Omair, A.H. Touny, F.A. Al-Odail, M.M. Saleh, Electrocatalysis 8 (2017) 340–350.
[65] S.J. Yao, S.K. Wolfson Jun, B.K. Ahn, C.C. Liu, Nature 241 (1973) 471–472.
[66] S.N. Azizi, S. Ghasemi, M. Derakhshani-mansoorkuh, Int. J. Hydrogen Energy 41 (2016) 2118–21192.
[67] R. Ojani, J.B. Raoof, S.R.H. Zavvarmahalleh, J. Solid State Electrochem. 13 (2009) 1605–1611.
[68] S. Kavian, S.N. Azizi, S. Ghasemi, Chin. J. Catal. 37 (2016) 159–168.
[69] S.N. Azizi, S. Ghasemi, F. Amiripour, Sens. Actuator B 227 (2016) 1–10.